

# Benchmarking virtual cell models for in-the-wild perturbation response

Xinjie Mao<sup>1,2,3\*</sup>, Songming Zhang<sup>1,4\*</sup>, Qianhong Wen<sup>1,5\*</sup>, Xiangyu Wen<sup>1,6\*</sup>, Kedu Jin<sup>1,7</sup>, Hao Wu<sup>1,8</sup>, Shuizhou Chen<sup>1,9</sup>, Yuqiang Li<sup>2</sup>, Lei Bai<sup>1</sup>, Qi Liu<sup>10</sup>, Ning Ding<sup>1,11</sup>, Siqi Sun<sup>1,8\*</sup> and Zhangyang Gao<sup>1\*</sup>

<sup>1</sup>Shanghai Artificial Intelligence Laboratory, <sup>2</sup>Shanghai Innovation Institute, <sup>3</sup>School of Life Sciences, Westlake University, <sup>4</sup>Faculty of Computer Science and Control Engineering, Shenzhen University of Advanced Technology, Shenzhen, <sup>5</sup>College of Information Engineering, Sichuan Agricultural University, <sup>6</sup>School of Electronics and Information Technology, Sun Yat-sen University, <sup>7</sup>School of Life Science and Technology, China Pharmaceutical University, <sup>8</sup>Research institute of intelligent complex systems, Fudan University, <sup>9</sup>School of Computer Engineering & Science, Shanghai University, <sup>10</sup>Shanghai Skin Disease Hospital, School of Medicine & Frontier Science Center for Stem Cell Research, Bioinformatics Department, School of Life Sciences and Technology, Tongji University, <sup>11</sup>Department of Electronic Engineering, Tsinghua University

Virtual cell (VC) models aim to predict cellular responses to any perturbations *in silico* and have emerged as a promising approach for drug discovery and precision medicine. Yet, a clear gap still remains: while models routinely reported impressive results on standard benchmarks, it is unclear whether their predictions are truly meaningful in practice. This is mainly due to limitations in current evaluation setups, which are often overly simplified or inconsistent, and do not reflect the complexity and variability of real biological systems. Here, we introduce a standardized and modular benchmarking framework for virtual cell prediction. Our framework evaluates diverse models under in-the-wild challenging scenarios, including unseen cell contexts, unseen perturbations, and cross-dataset generalization, which better reflect practical applications. Our analysis shows that model performance is highly context-dependent and shaped by task design and evaluation criteria. In commonly used setups, performance is often overestimated, and naive dataset aggregation can even reduce performance. When evaluated under more strict conditions, model performance drops markedly, indicating limited robustness to shifts across cellular contexts. In unseen perturbation settings, models including simple linear approaches capture global transcriptional trends but fail to recover fine-grained perturbation-specific effects. In addition, different evaluation metrics focus on different biological properties, leading to substantially different model rankings. Together, our framework provides a more reliable and biologically grounded evaluation, offering clearer guidance for applying virtual cell models in real scenarios.

## 1. Introduction

Virtual cell (VC) models aim to predict cellular responses to genetic or chemical perturbations *in silico* and have emerged as a powerful paradigm for studying gene function and drug response. These approaches are closely linked to single-cell perturbation experiments, which enable systematic characterization of cellular responses to targeted interventions. High-throughput platforms such as Perturb-seq [1, 2], CROP-seq [3], and chemical screens like sci-Plex [4], built upon genome-scale CRISPR screening technologies [5, 6], enable parallel profiling of hundreds of perturbations at single-cell resolution, supporting gene function analysis and drug response characterization [7–9]. Despite these advances, experimental coverage remains limited relative to the vast combinatorial perturbation space [10, 11]. This gap has driven the development of computational approaches for VC prediction under unmeasured perturbations, cell states, and experimental conditions [12, 13].

However, robust perturbation prediction remains challenging. Cellular responses are highly context-dependent, varying across cell types and genetic backgrounds, and perturbations often interact in nonlinear ways, especially in combinatorial settings. In addition, datasets generated by different platforms or laboratories exhibit substantial technical variation, complicating cross-dataset generalization. Existing benchmarks are limited in scope and often rely on model-specific implementations with

◆: Core Contributor   ◆: Corresponding Author

Please send correspondence regarding this report to sunsiqi@pjlab.org.cn; gaozhangyang@pjlab.org.cn

inconsistent preprocessing, training protocols, and evaluation settings, leading to fragmented and potentially unfair comparisons [14, 15]. As a result, it remains unclear which models truly capture biologically meaningful perturbation responses, rather than merely fitting global transcriptional trends [16, 17].

A range of modeling strategies has been proposed, including VAE-based generative models such as scGen [18], scVI [19], trVAE [20] and CPA [21], optimal-transport-based methods such as CellOT [22, 23], gene-regulatory approaches like GEARS [24], diffusion-based models such as Squidiff [25], and transformer-based methods leveraging pretrained embeddings like scGPT [26], scFoundation [27], Geneformer [28], and scBERT [29]. While these approaches demonstrate that perturbation responses can be learned from data, their robustness under realistic generalization settings remains unclear. Reported performance often drops in unseen cell types, new perturbations, or cross-dataset scenarios. Existing benchmarks are limited in scope and typically depend on original model implementations, leading to inconsistent pipelines and fragmented comparisons [14, 15, 30–33]. Importantly, while several studies have reported that simple linear models can perform competitively in certain settings [16, 17, 34], it remains unclear under which conditions these models break down. In particular, it is not well understood whether they capture biologically meaningful perturbation-specific effects, or primarily reflect global transcriptional trends. This distinction is critical for biological interpretation.

To address these issues, we introduce a standardized and modular benchmarking framework for single-cell perturbation modeling. Our framework integrates diverse models under consistent input–output interfaces, enabling controlled comparison and flexible adaptation of model components. Unlike prior benchmarks that merely rely on random splits, our framework focuses on *in-the-wild* generalization, evaluating models under realistic conditions where cellular contexts and perturbations are not observed during training. We explicitly disentangle different out-of-distribution scenarios, including unseen cell contexts, unseen perturbations, and cross-dataset integration, which together approximate real experimental settings. This combination of modular design and *in-the-wild* evaluation enables systematic analysis of model behavior and provides a more biologically grounded assessment of virtual cell models.

Across these settings, we find that model performance is highly context-dependent and shaped by task design, representation, data integration, and evaluation criteria. Task design strongly influences model behavior: (1) Embedding-defined unseen-cell splits are substantially more challenging than random splits, revealing limited robustness to shifts across cellular contexts; (2) Model performance further depends on how perturbation effects are represented. While many models, including simple linear approaches, can capture global transcriptional shifts, they often fail to accurately quantify perturbation-specific responses, particularly under distribution shifts or in combinatorial settings; (3) Cross-dataset integration remains a major challenge. Even datasets from the same study can differ markedly in count-level distributions, and naive aggregation strategies often degrade performance, indicating that dataset heterogeneity is a central obstacle; (4) Evaluation metrics capture distinct biological aspects of perturbation responses, and model rankings vary accordingly. Together, these findings highlight the importance of moving beyond global transcriptional similarity when evaluating perturbation models and provide a foundation for more reliable and biologically meaningful assessment of cellular responses.

## 2. Results

### 2.1. Benchmarking framework for virtual cell prediction

**Scenarios** To better support biologists in assessing virtual cell model reliability for practical applications, we developed a comprehensive benchmark framework, including state-of-the-art methods,

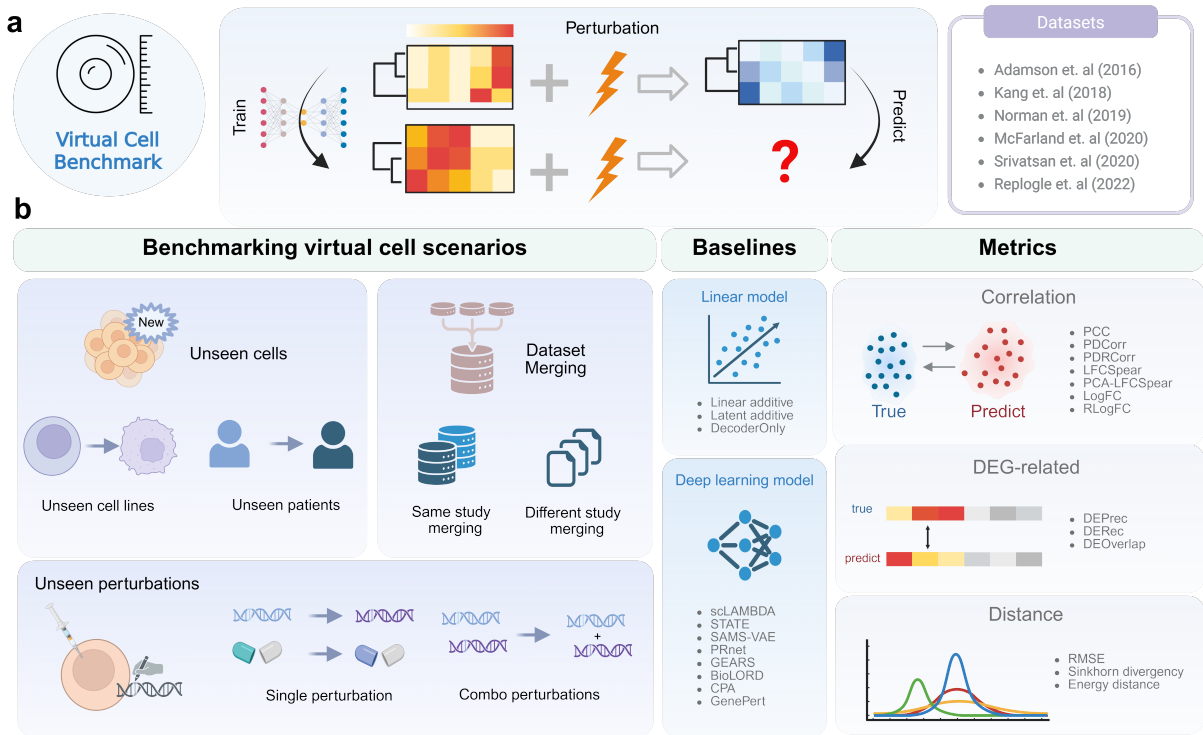


Figure 1 | **Overview of benchmarking workflow, methods in VCBench.** (a) A schematic illustration of the virtual cell prediction. Virtual cell model takes as input the pre-perturbation cellular state, including gene expression profiles and optional context such as cell type or perturbation identifiers (e.g., gene knockout or drug treatment). The goal is to predict the post-perturbation gene expression, capturing both global shifts and gene-level responses. (b) We classify virtual cell prediction into three scenarios: unseen cells generalization, unseen perturbation generalization, and multi-dataset merging. Under each setting, we benchmark 11 representative methods across 7 widely used datasets from 6 representative studies, while using 3 categories of metrics for a comprehensive comparison.

diverse datasets, and rigorous evaluation metrics (Fig. 1). In this study, we evaluate models under three key scenarios that better reflect real-world generalization challenges.

- *Unseen cells generalization scenario.* Unseen cells generalization refers to the ability of a model to predict gene expression for cell line or donor states that are not observed during training, which is often required in real applications where models must transfer to new cellular contexts. Previous random splits can mix highly similar cells across training and test sets, which weakens the difficulty of evaluation. This setting does not sufficiently reflect real applications where models must transfer to new cellular states. We therefore construct evaluation splits that explicitly remove overlap in cellular context to better test generalization to unseen cells.
- *Unseen perturbation scenario.* Predicting responses to perturbations not observed during training is a fundamental requirement for practical applications. However, experimental coverage of perturbation space is inherently limited, making it necessary for models to extrapolate beyond seen conditions. In this setting, we evaluate model performance on both single and combinatorial perturbations, covering diverse intervention types such as genetic and chemical perturbations.
- *Multi-dataset merging scenario.* Although large-scale datasets are increasingly available, most

models are trained within individual studies, limiting their ability to leverage broader data diversity. Integrating datasets offers the potential to improve generalization, but is challenged by differences in gene coverage, sequencing depth, and distribution shifts across studies. We therefore test whether models can effectively utilize merged datasets while maintaining robust performance under varying experimental conditions.

**Methods and datasets** We compare a total of 8 deep learning methods, including scLAMBDA, SAMS-VAE, PRNet, GEARS, BioLORD, CPA, STATE and GenePert. These models learn nonlinear mappings from input gene expression together with perturbation or context information to the target cellular response. Their designs differ substantially, ranging from variational formulations and latent generative models to perturbation-conditioned neural architectures. Given growing concerns in recent studies that complex deep learning models may offer only limited improvement over simpler approaches, we further include 3 baseline models: Linear Additive, Latent Additive, and DecoderOnly, as well as a foundation model, STATE.

We conduct experiments on approximately 7 publicly available perturbation datasets curated from scPerturb [35], including 6 representative studies such as McFarland2020 [36], Kang2018 [37], AdamsonWeissman2016 [2], Norman2019 [38], ReplogleWeissman2022 [11], and SrivatsanTrapnell2020 [4]. All methods are evaluated on these datasets under a unified experimental framework. Within this framework, we integrate a wide range of perturbation models under a unified interface with preserving each original implementation. The design preserves original implementations while standardizing inputs and outputs, enabling fair comparisons and supporting controlled ablation studies on key components such as covariates.

**Metrics** We evaluate model performance using multi-level metrics, including *correlation-based measures* (PCC, PDCorr, PDRCorr, LFCspearman, PCA-LFCspearman, LogFC, and RLogFC), *distribution-level distances* (RMSE, Sinkhorn divergence, and energy distance) [39–41], and *differentially expressed gene (DEG)-related scores* (DEPrec, DERec, and DEOverlap). This multi-level design is motivated by the nature of perturbation response prediction, where accurate modeling requires not only matching gene-wise correlations, but also preserving global expression distributions and recovering biologically meaningful differential signals.

- Correlation-based metrics quantify gene-level agreement between predicted and true responses, capturing whether perturbation-induced expression changes are correctly ranked and directionally consistent.
- DEG-related metrics explicitly evaluate the recovery of differentially expressed genes, which are central to biological interpretation in perturbation experiments [14, 42]. These genes reflect direct and indirect regulatory effects of perturbations, and accurate recovery is essential for downstream pathway analysis and mechanistic interpretation. Together, these metrics disentangle complementary aspects of prediction quality under perturbation-induced distribution shift, enabling a fine-grained evaluation of model behavior in realistic biological settings.
- Distribution-level distances further assess whether the predicted cellular state matches the global shift in expression space induced by perturbations.

## 2.2. Benchmarking analysis for the unseen-cell generalization scenarios

A central challenge in unseen cell generalization scenarios is whether current benchmarks truly reflect their ability to generalize to previously unobserved cellular contexts. In particular, conventional random splits may substantially underestimate task difficulty, as transcriptionally similar cells can be

shared between training and test data [14, 43]. To address this limitation, we construct training and test sets using single-cell foundation model (scFM) embeddings, where splits are defined based on cell-state similarity (Fig. 2a, Fig. S1). Specifically, cells are grouped in the pretrained scFM latent space, and training–test splits are constructed based on clustered representation similarity to ensure separation of closely related cell states.

As shown in Fig. 2b, the scFM-based strategy produces more structured and separated partitions compared to random splitting, particularly for unseen cell lines in McFarland2020 [36] (Fig. S2). Consistent with these embedding differences, model performance decreases across nearly all methods under the scFM-based split relative to the random split (Fig. 2c). Also, all model performance across evaluation metrics is generally limited, indicating that accurate prediction for unseen-cell generalization remains challenging while random splitting can make models look more robust than they actually are. (Fig. 2d).

Clear differences in relative model capability are observed. Without scFM cell embeddings, linear additive models, BioLORD and scLAMBDA consistently achieve the strongest overall performance across multiple metrics, forming a clear top-performing group. In addition, among models that support scFM cell embeddings, BioLORD remains the better performance, suggesting that it can make effective use of auxiliary contexts while preserving robustness under hard conditions (Fig. 2d). These results highlight that robustness, rather than model complexity alone, is critical for performance under hard unseen-cell conditions.

We also evaluate the impact of incorporating scFM cell embeddings across different models (Fig. 2e). Notably, STATE still gains from cell embeddings under both settings, suggesting that its architecture can effectively exploit cell-state information beyond simple interpolation. In contrast, models such as CPA and BioLORD show limited gains in both settings, indicating that their design limits how much they can leverage external cell representations. Overall, cell embeddings do not lead to uniform improvements, but instead provide selective gains that depend on both the split setting and model architecture.

In the unseen patient setting (Kang2018 [37]), the distribution shift between training and test data is relatively small, as shown in Fig. 2b, where different partitions remain close in latent space. Consistent with this, most models achieve strong performance across evaluation metrics (Fig. 2f, Fig. S3), indicating that unseen-cell generalization is more achievable when distribution differences are limited. Despite the reduced difficulty, linear additive models, BioLORD, and scLAMBDA maintain stable performance, consistent with their behavior in the more challenging cell-line setting.

In summary, the benchmark analysis of the unseen cell generalization scenario yields the following key findings: (1) Embedding-based splits better reflect real unseen-cell challenges, and performance drops across most models. (2) Linear additive models, BioLORD, and scLAMBDA show the most stable performance across different shift levels. (3) Cell embeddings extracted from scFM are most effective when models need to extrapolate across cell-state distributions.

### 2.3. Benchmarking analysis for the unseen-perturbation generalization scenarios

In the unseen perturbation generalization scenario, we evaluate whether models can extrapolate the effects of perturbations that are absent during training while keeping the cellular context fixed. To systematically assess this capability, we consider two primary datasets: (1) Genetic perturbations are evaluated on the ReplogleWeissman2022-essential screen, which measures single-gene CRISPR knockouts in K562 cells. (2) Chemical perturbations are evaluated on the SrivatsanTrapnell2020 Sciplex3 dataset with fixed dosage and time effects (10  $\mu$ M, 24 hours).

In addition, prior evaluations of perturbation prediction have suggested that a simple linear baseline

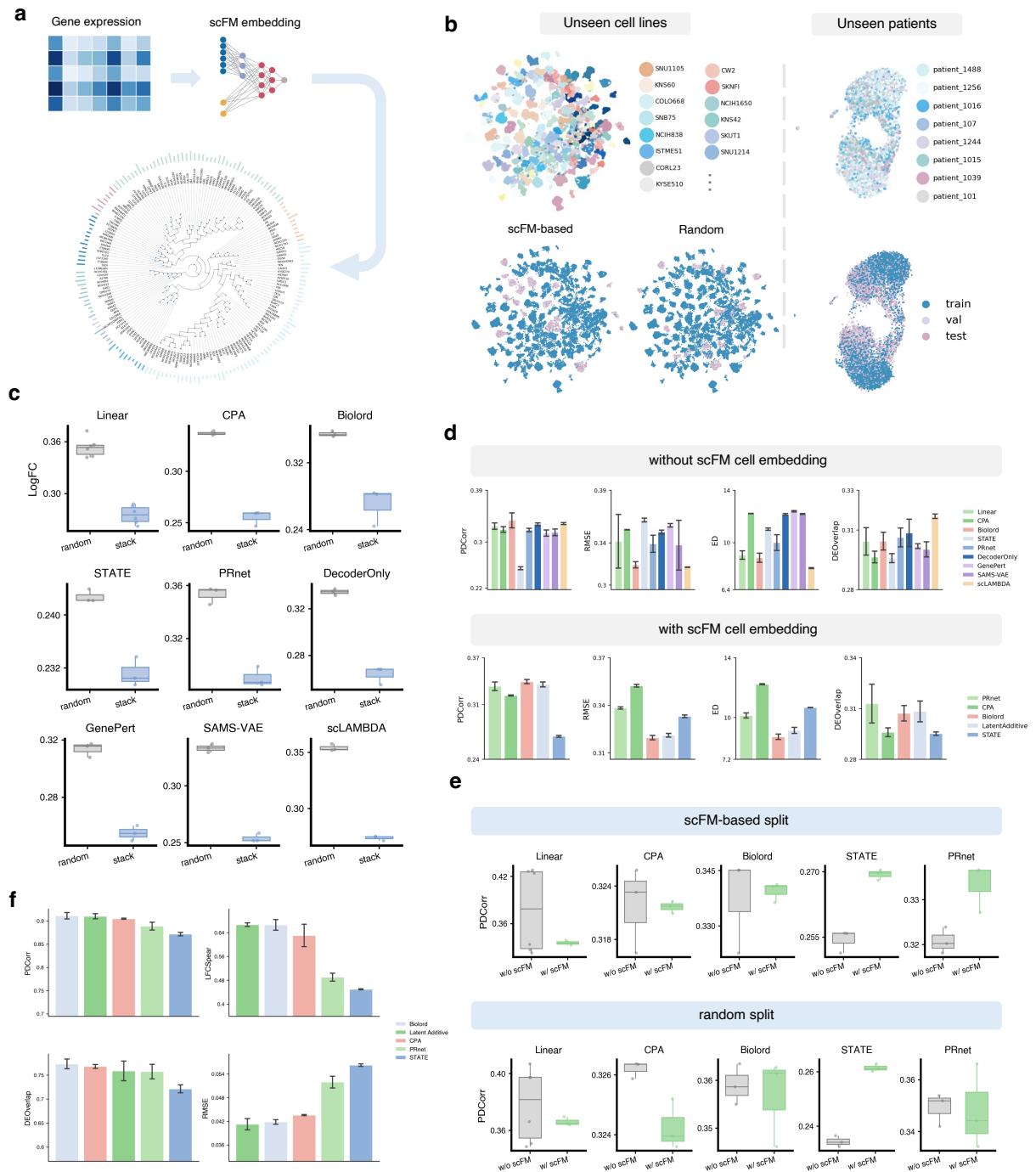


Figure 2 | Unseen-cell evaluation under scFM-based and random splitting strategies. (a) Construction of unseen-cell splits using scFM-derived cell representations. Control-cell expression profiles are projected into a foundation model embedding space to define partitions based on cell-state similarity. (b) Visualization of unseen cell-line and unseen patient splits under scFM-based and random partitioning strategies. (c) Comparison of model performance under random and scFM-based splits across evaluation metrics. (d) Model performance across representative metrics without and with scFM cell embeddings. (e) Model-wise comparison of performance with and without scFM cell embeddings under different splitting strategies. (f) Performance comparison across unseen patient settings.

often outperforms more complex deep learning or foundation models such as STATE [16, 17, 32]. However, such evaluation protocols have mainly relied on global reconstruction metrics, without sufficiently considering biologically meaningful criteria, particularly those aligned with practical questions studied by biologists. For example, accurately recovering the direction and relative ranking of top DEGs, which are critical for interpreting functional responses, is often overlooked. To address this limitation, we incorporate additional analyses centered on Top HVGs and DEG-related metrics, enabling a more comprehensive assessment of model performance from both global reconstruction and biologically relevant perspectives.

**Genetic perturbation generalization.** To evaluate model performance on unseen genetic perturbations, we constructed four test splits for detailed evaluation under progressively different perturbation compositions. From a distributional perspective, after constructing the training and test splits, we compute the energy distance between the training split and each of the four test splits to quantify the magnitude of the shift. The resulting distances show an ordering with increasing difficulty across the four test settings: Single Unseen, Combo Unseen 0, Combo Unseen 1, and Combo Unseen 2 (Fig. 3a). Notably, the final model performance exhibits the same ordering pattern (Fig. 3b). This suggests that test splits with smaller distribution shifts relative to the training set tend to yield higher performance, while larger shifts are associated with performance drops.

Across HVG-based metrics, linear additive baselines are consistently weaker than more expressive deep models such as SAMS-VAE (Fig. 3b). This indicates that perturbation effects are not well described by a simple additive transformation in expression space. STATE achieves relatively weak results, which may be related to the limited scale of the Norman dataset and its model capacity [44]. Beyond global HVG-based metrics, we also evaluate DEG-based metrics, which mainly assess the ability to recover perturbation-responsive genes. Specifically, we consider the top 50 DEGs with opposite regulation directions and compute the accuracy of correctly identifying up- and down-regulated genes, providing a more direct measure of whether the model captures biologically consistent perturbation responses (Fig. 3c–d). Notably, PRnet shows lower performance on the top 2,000 HVGs, but maintains the most stable performance on DEG-related evaluation. This difference indicates that strong performance on the full HVG space does not necessarily imply strong performance over DEGs, and vice versa. This may arise because global HVG-based metrics emphasize overall expression trends, which can obscure perturbation-specific signals captured by DEG-based metrics.

**Chemical perturbation generalization.** We next focus on chemical perturbations to examine whether these observations remain consistent under compound-induced responses. Fig. 3e shows the overall results on three cell lines for the unseen chemical perturbation task. CPA, BioLord, and Latent Additive achieve the better PDCorr and LFCspear performance overall, consistently ranking among the top three models across different cell lines and metrics. In contrast, methods such as Linear Additive, GenePert, DecoderOnly, and SAMS-VAE show clear performance drops across all three cell lines, suggesting that simple additive assumptions or weaker latent modeling are insufficient for robust cross-cell-line generalization.

For more detailed analysis, we conduct more analysis on Top DEGs of Sciplex3 dataset, K562 cell line, Andarine perturbation. As shown in Fig. 3f, energy distance results are coarse, and PCC results shows the differences of 3 models. But in general, most PCC values of DEGs are between  $-0.1$  and  $0.1$ . This shows these deep learning models are unable to accurately approximate the true value after perturbation [42, 45]. For the biology application of these deep learning models, the direction of gene expression level changes is most important, rather than the exact value. As Fig. 3g shows, most of the predictions of the direction of top 20 DEGs are true, but these models are hard to approximate the exact value.

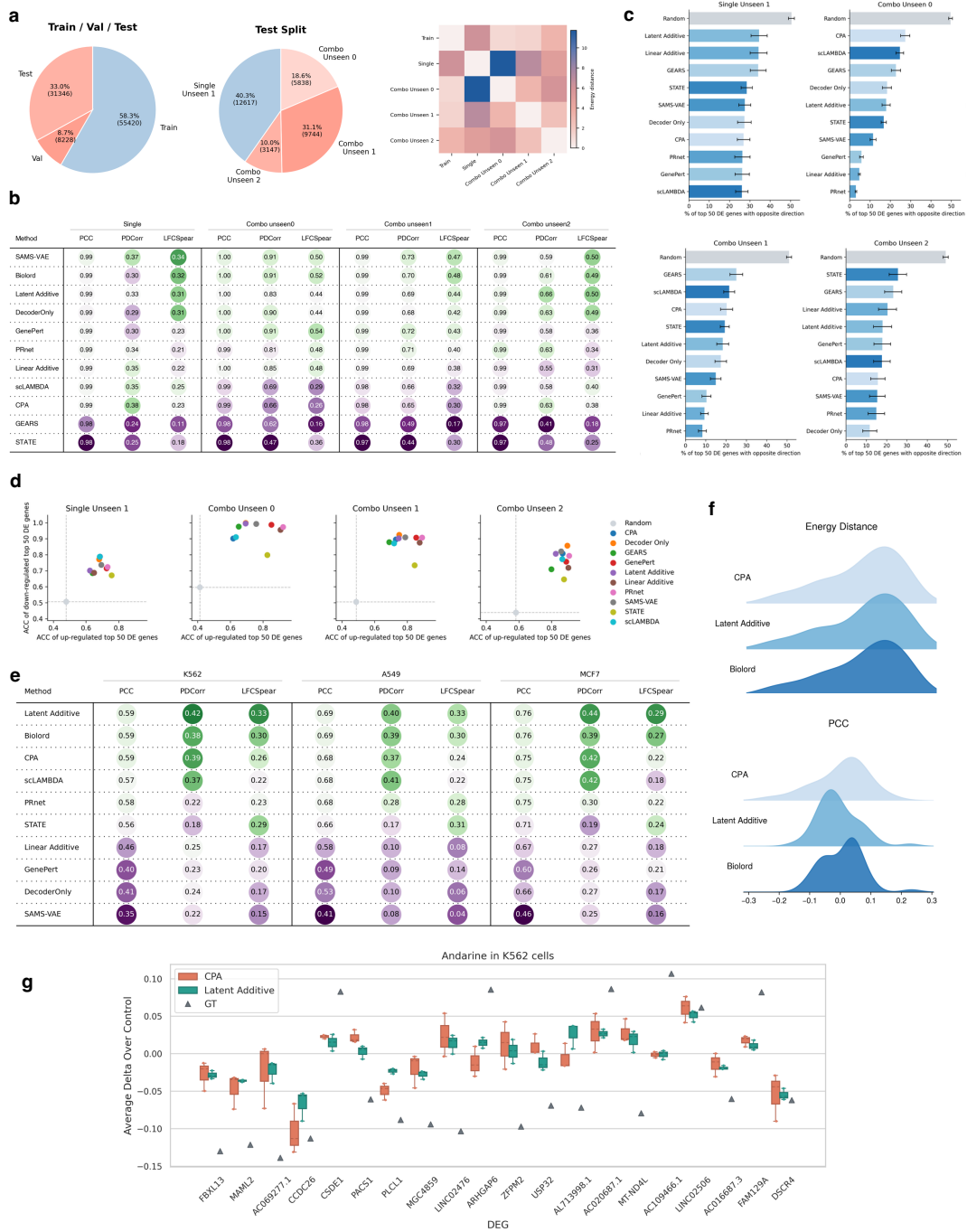


Figure 3 | **Unseen perturbation task results.** (a) Data properties of the Norman[38] dataset. Left: data split used for the combinational perturbation task. Right: energy-distance heatmap between the perturbation embedding sets of the four test splits and the training split. (b) Results of all models on *Combo Unseen* task. (c) Top-50 DEG opposite-direction ratio of all models. The ratio is computed using the standard DEG computation procedure rather than the modified version used in DEOverlap. Lower is better. (d) Mean accuracy of predicted up-regulated DEGs versus mean accuracy of predicted down-regulated DEGs. Points closer to the top-right corner indicate better performance. (e) Results of all models on the *Single Unseen* task. (f) For each gene of the Top 50 DEG, we first compute the energy distance (**top**) and PCC (**bottom**) between the predicted cell set and the ground-truth cell set, and then plot the corresponding probability density distributions. (g) Delta-over-control expression of the top 20 DEGs.



Overall, chemical perturbation results are consistent with genetic perturbation findings: while several models can capture global expression changes, their ability to accurately quantify and precisely fit key gene expression values remains limited. Moreover, reliable evaluation requires biologically meaningful metrics such as DEG prediction, rather than relying solely on global reconstruction.

## 2.4. Benchmarking analysis for cross-dataset integration

Integrating datasets across conditions provides a natural way to increase both scale and diversity, especially in data-limited settings; however, it remains unclear whether such aggregation consistently improves generalization performance [43]. We study how different dataset integration strategies affect gene-space alignment and perturbation prediction under cross-dataset settings, focusing on highly variable genes (HVGs) selection, normalization, and merging behavior across scales and studies. Specifically, we evaluated linear additive, CPA, BioLORD, and scLAMBDA models on multiple K562 CRISPR perturbation datasets, including Adamson10X001 [2], Adamson10X010 [2], and ReplogleK562 [11]. Adamson10X001 and Adamson10X010 originate from the same study, while ReplogleK562 provides a cross-study dataset for evaluating merging under heterogeneous experimental conditions (Fig. 4a). All models were evaluated without incorporating scFM-extracted cell embeddings.

We first examine how restricting datasets to HVGs affects alignment. When using all genes, gene overlap between datasets is highly asymmetric, even for datasets measured in the same cell line, reflecting differences in gene coverage across studies. Restricting each dataset to its top 2,000 HVGs substantially reduces this discrepancy, resulting in a more comparable and balanced overlap of effective feature space (Fig. S4, Fig. 4c, top). This suggests that HVG selection provides a simple but effective way to partially harmonize feature space across datasets in cross-study settings [46].

We next analyze how count-level normalization affects expression distributions. Systematic differences in per-cell transcript counts are observed across datasets prior to scaling (Fig. 4b). A simple per-cell count scaling reduces these global shifts, which is associated with consistent performance gains across evaluation metrics when aggregating the full test set.

We then investigate how the order of HVG selection and dataset merging affects performance (Fig. S5). Selecting HVGs before merging (merge-after) improves correlation-based metrics such as PDCorr, indicating better preservation of perturbation-related signals within each dataset. In contrast, selecting HVGs after merging (merge-before) reduces distributional distance measures such as Sinkhorn divergence and RMSE, indicating improved global alignment of expression distributions (Fig. 4c, bottom).

We further study the effect of same-study merging effects using Adamson10X001 (smaller dataset) and Adamson10X010 (larger dataset). For the smaller dataset, merging provides modest improvements over single-dataset training, while for the larger dataset, gains are negligible (Fig. 4d). This indicates that merging is more beneficial when the original dataset provides limited coverage of the underlying distribution. Finally, we analyze cross-study merging effects under a controlled setting, which uses a consistent merge-after strategy and subsample ReplogleK562 to match the size of Adamson10X010 to remove scale effects (Fig. 4e). Even under matched sizes, merging leads to smaller performance degradation on ReplogleK562 than on Adamson10X010, suggesting that dataset identity itself strongly influences integration behavior.

Overall, these results indicate that merging outcomes depend on intrinsic biological variation, leading to context-dependent effects in the integration of multiple datasets.

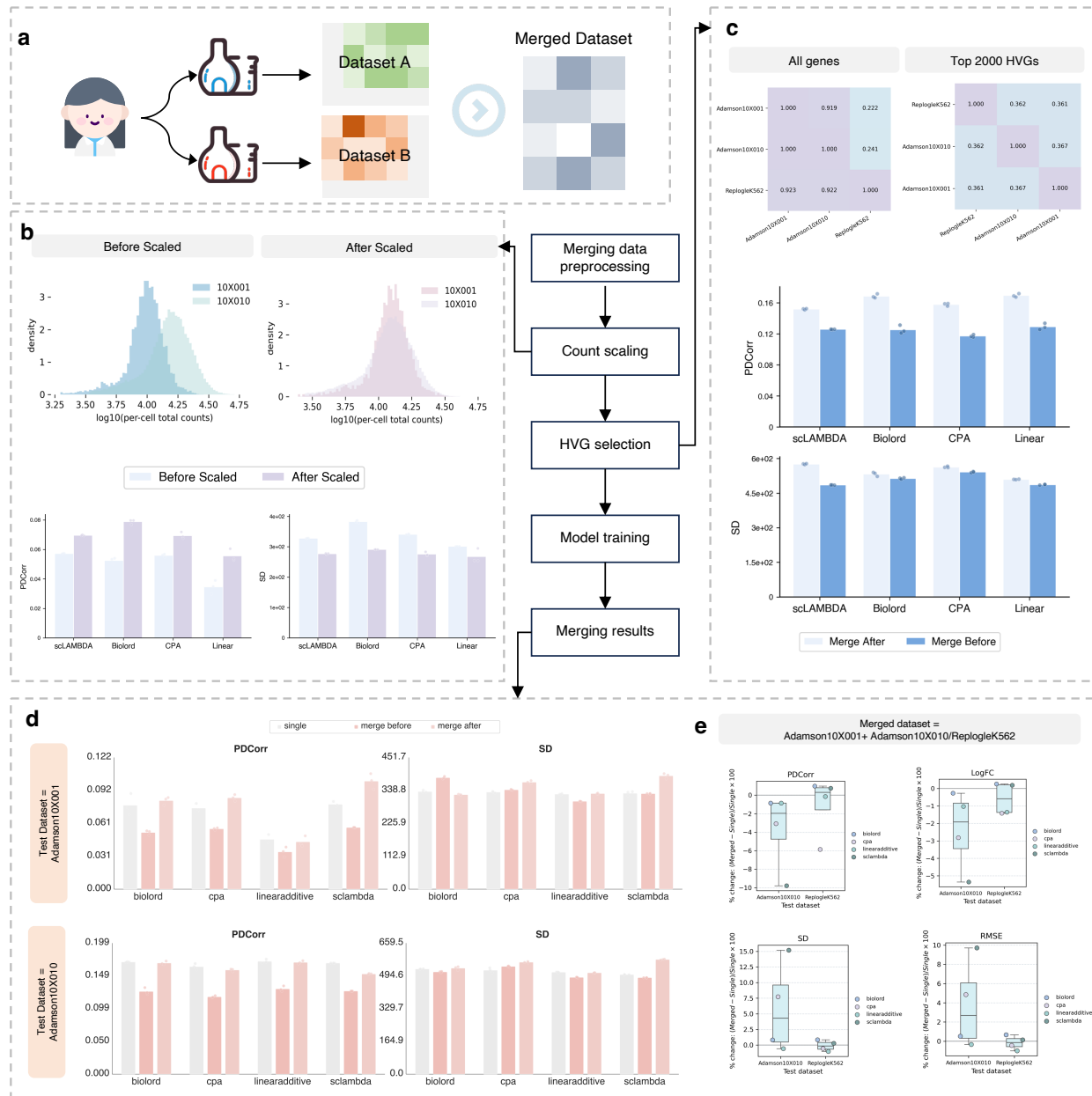


**Figure 4 | Cross-dataset integration under different preprocessing, merging, and evaluation settings.** (a) Overview of the dataset merging workflow, including merging preprocessing, count scaling, HVG selection, model training, and evaluation. (b) Per-cell count distributions before and after count scaling for Adamson10X001 and Adamson10X010, together with model performance before and after scaling. (c) Gene overlap matrices using all genes and top 2000 HVGs, and model performance under different HVG selection strategies (merge-before and merge-after). (d) Model performance comparison on the Adamson10X001–Adamson10X010 dataset pair under single-dataset training, merge-before, and merge-after settings, evaluated separately on Adamson10X001 and Adamson10X010. (e) Model performance under the merge-after strategy for merged datasets containing Adamson10X001 with either Adamson10X010 or ReplogleK562, evaluated on Adamson10X010 and ReplogleK562 as test datasets.

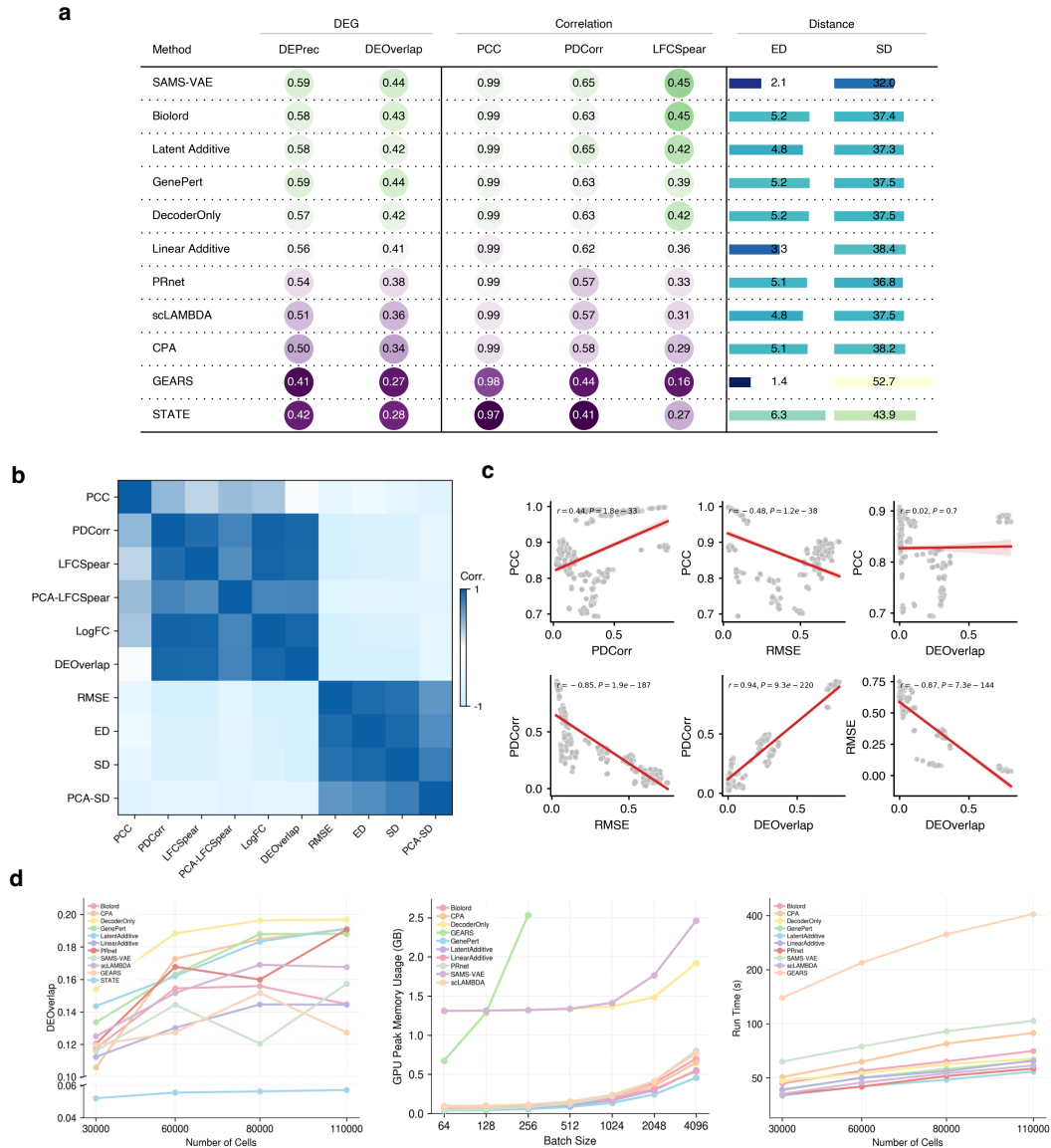


**Figure 5 | Metric-dependent evaluation reveals complementary aspects of model performance and computational trade-offs.** (a) Model performance across representative evaluation metrics, grouped into DEG-related, correlation-based, and distribution-level distance measures. (b) Correlation matrix of pairwise evaluation metrics. (c) Pairwise relationships between representative metrics, illustrating consistency within metric groups and divergence across different evaluation dimensions. (d) Computational efficiency analysis, including performance trends with increasing dataset size, GPU memory usage with batch size, and runtime scaling across models.

## 2.5. Robustness assessment of evaluation metrics

Accurately evaluating virtual cell models remains challenging because different metrics capture fundamentally different aspects of model behavior. Metrics that perform well in measuring mean-level agreement may fail to reflect biologically meaningful perturbation signals or distribution-level consistency [35, 41]. As a result, relying on a single metric can lead to incomplete or even misleading conclusions. Therefore, we analyzed performance across a panel of evaluation metrics spanning complementary aspects of perturbation prediction. Rather than relying on a single metric, we grouped evaluation criteria into three categories: correlation-based metrics, DEG-related metrics, and distribution-level distance measures.

Model performance shows strong dependence on the choice of evaluation metric (Fig. 5a). While most models achieve similarly high values under PCC, indicating strong agreement in global expression profiles, this metric shows limited discriminative power across other metrics. Consistently, PCC shows weak correlation with other metrics in the correlation heatmap (Fig. 5b), further indicating its limited suitability for evaluating perturbation prediction tasks. In contrast, perturbation-focused metrics such as PDCorr, and DEG-related measures exhibit greater variation and more clearly separate model performance.

In addition to predictive performance, models differ substantially in computational efficiency (Fig. 5d). Simpler models, such as linear approaches, exhibit low GPU memory usage and stable runtime scaling with increasing data size. In contrast, more complex deep learning models require substantially higher memory and show steeper increases in runtime as dataset size and batch size grow. These results highlight that model selection involves not only predictive accuracy but also computational considerations, particularly in large-scale settings. Together, they underscore the need for evaluation frameworks that account for both performance and practical constraints.

## 3. Discussion

In this study, we systematically evaluated perturbation prediction models across multiple generalization scenarios under a unified benchmarking framework. Overall, our results show that while most models capture global expression shifts, which reflect broad transcriptional responses to perturbations, their ability to precisely quantify perturbation-specific effects remains limited, particularly for simpler linear approaches. Model performance further depends strongly on task design, data characteristics, and evaluation criteria, highlighting the need for user-specific, task-dependent model selection [14, 15], as summarized in Fig. 6.

We summarize the main findings and their practical implications as follows (Fig. 6). These observations collectively indicate that model performance is inherently context-dependent and cannot be reliably assessed using a single model or metric.

- Within single-dataset settings, we considered both unseen-cell and unseen-perturbation scenarios (Fig. 6). In unseen-cell generalization, stricter evaluation protocols substantially reduce performance across all models, indicating limited robustness to distribution shifts across cellular contexts. Under these conditions, simpler or more stable models, including linear additive approaches, BioLORD, and scLAMBDA, tend to perform more consistently. Unseen perturbation prediction introduces a different challenge, where performance depends strongly on how perturbation effects are represented. Simple additive models perform poorly in these settings, despite their strong performance in capturing global expression trends. This suggests that linear assumptions are insufficient for modeling perturbation-specific effects. In contrast, structured approaches such as BioLORD and CPA generalize more reliably. For more complex settings, in-

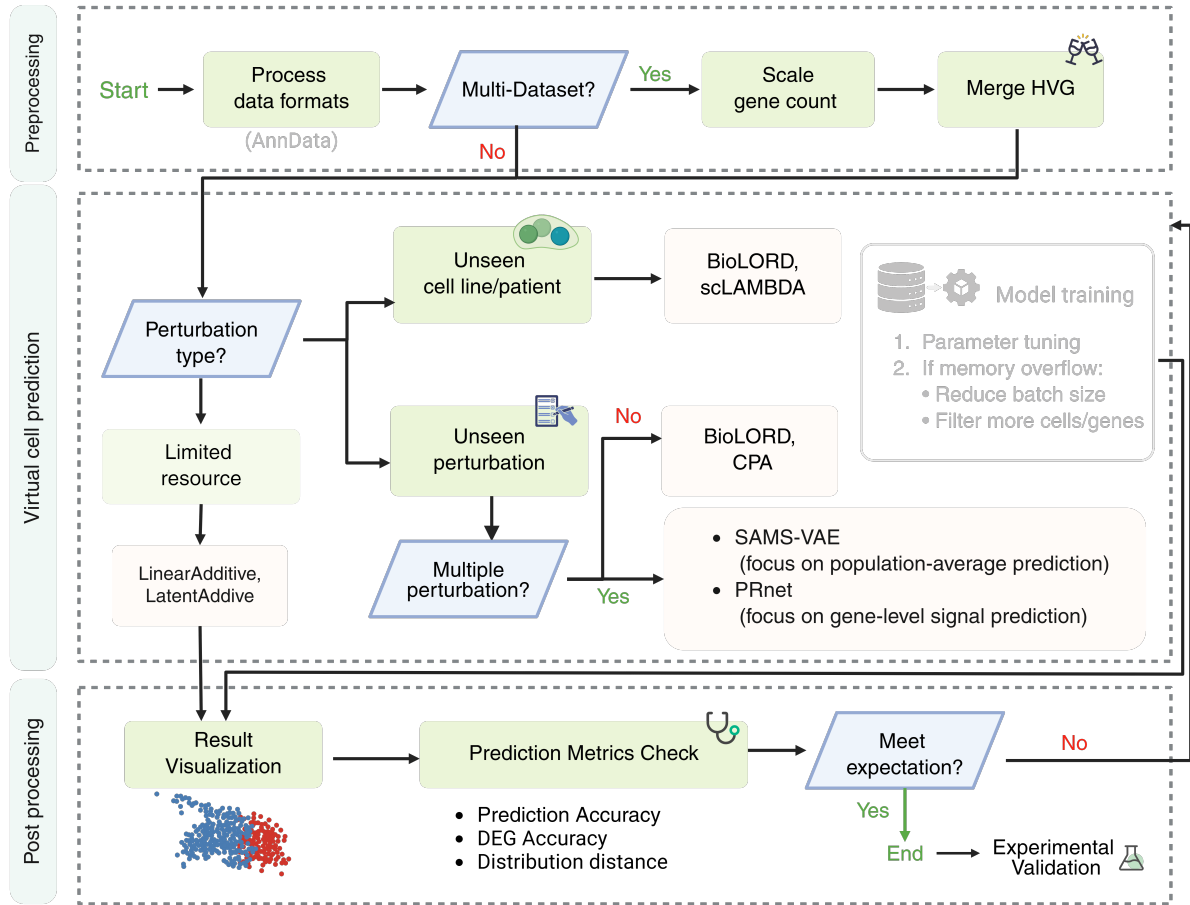


Figure 6 | A step-by-step guide for virtual cell prediction is organized into three stages. Before training, users standardize input data, including quality control, gene-level normalization, and optional cross-dataset alignment when multiple datasets are used to ensure a consistent feature space. During the VC modeling stage, users select models based on the task setting (e.g., unseen cell states or perturbation conditions) and computational limits. Methods ranging from linear baselines to representation learning and generative models are tested sequentially, with standard hyperparameter tuning. If resource issues occur, users may reduce batch size or model complexity; if unresolved, switch to alternative methods. After prediction, results are evaluated using both qualitative inspection and quantitative metrics covering correlation, distribution consistency, and DEG recovery. If performance is satisfactory, downstream analysis is performed; otherwise, users return to model selection and try other VC methods.

cluding combinatorial perturbations, models such as SAMS-VAE or PRNet may provide additional advantages.

- In cross-dataset settings, integrating datasets introduces additional complexity beyond scaling data size. Performance depends on dataset compatibility. This may reflect differences in experimental conditions, perturbation design, and biological context. As a result, naive aggregation can lead to degraded results. As illustrated in Fig. 6, preprocessing plays a critical role, particularly in feature-space alignment and normalization. The observed sensitivity to HVG selection further suggests that models are not invariant to input space differences.
- Across all scenarios, evaluation metrics critically shape model comparison. Metrics capturing global expression similarity show limited discrimination, whereas perturbation-focused and distribution-level measures reveal larger differences, indicating that model performance is inherently multi-dimensional.

Beyond differences in model ranking, the benchmark reveals three recurring bottlenecks that limit reliable generalization. First, current models lack expressive and transferable representations. Linear models can capture global expression shifts, but they fail to quantify perturbation-specific effects, especially under distribution shifts or complex perturbations. This reflects a gap between fitting average trends and modeling biologically meaningful responses. Across both unseen-cell and unseen-perturbation settings, models often rely on local similarity or simple structural assumptions, rather than learning representations that generalize across cell states and perturbation conditions. Second, cross-dataset integration remains a fundamental challenge. The difficulty of merging datasets is not explained by scale alone [13, 43]. Performance often degrades even after alignment procedures. This suggests that current methods cannot consistently learn across heterogeneous studies, making cross-dataset generalization a central limitation rather than a simple data-scaling issue. Third, different metrics capture distinct biological aspects of perturbation responses. Metrics based on global expression similarity are sufficient for assessing overall transcriptional shifts, but they provide limited insight into perturbation-specific effects. In contrast, perturbation-focused metrics, such as differential expression consistency, better identify biologically meaningful responses, while distribution-level metrics capture cell-to-cell heterogeneity. The choice of metric should therefore be guided by the biological question. Global metrics are suitable for assessing overall transcriptional trends, DEG-related metrics help identify key responsive genes, and distribution-level metrics capture cellular heterogeneity.

However, this study has several limitations. The analysis is restricted to currently available perturbation datasets, and the results may depend on the specific studies included. Differences in experimental design and perturbation coverage may also affect the observed patterns. Although we evaluated a representative set of models, the space of possible architectures is broader. In particular, only a limited set of scFM representations was considered, which may influence conclusions about the role of cell-state embeddings [27–29]. The cross-dataset analysis focuses on selected representative datasets. While this allows for a controlled comparison, it is unclear how well the results generalize to a wider range of datasets. Finally, we did not systematically examine additional covariates such as dosage and time. These factors are known to affect perturbation responses and may also influence model performance.

Looking ahead, advancing perturbation prediction will require both improved data resources and stronger representation learning. Expanding larger perturbation datasets under consistent experimental settings will be important [13, 47, 48], along with more robust strategies for integrating heterogeneous datasets. A key direction is to develop modeling frameworks that explicitly handle heterogeneity across cell states, perturbations, and datasets, rather than relying on shared representations learned from pooled data. In this context, multi-scale and multi-modal foundation models offer a promising direction [26, 27, 49], but their impact will depend on how effectively they are

Table 1 | Summary of datasets used in the benchmark.

Dataset	Generalization	#Cells	Covariates
McFarland2020 [36]	Cells	48,310	170 cell lines
Kang2018_CD4Tcells [37]	Cells	11,238	8 patients
AdamsonWeissman2016_10X001 [2]	Dataset	5,752	1 cell line
AdamsonWeissman2016_10X010 [2]	Dataset	56,380	1 cell line
Norman2019 [38]	Perturbation	106,849	1 cell line
ReplogleWeissman2022_K562 [11]	Perturbation	152,915	1 cell line
SrivatsanTrapnell2020_sciplex3 [4]	Perturbation	164,771	3 cell line

Dataset	Perturbation Type	Setting	#Perturbations
McFarland2020	Drug	Single	3
Kang2018_CD4Tcells	Cytokine	Single	1
AdamsonWeissman2016_10X001	Gene	Single	7
AdamsonWeissman2016_10X010	Gene	Single	73
Norman2019	Gene	Combo	226
ReplogleWeissman2022_K562	Gene	Single	499
SrivatsanTrapnell2020_sciplex3	Drug	Single	187

integrated into downstream prediction models.

## 4. Methods

### 4.1. Benchmark Datasets

We selected 7 widely used single-cell perturbation datasets from the processed release of scPerturb [35], which provides harmonized AnnData objects and standardized metadata across studies. Together, these datasets cover the benchmark scenarios studied here: unseen-cell generalization, unseen-perturbation generalization, and cross-dataset integration. They also span multiple perturbation modalities, including genetic, chemical, and cytokine perturbations, and include both single-perturbation and combinatorial settings. This diversity allows us to evaluate model robustness under a range of biologically and technically realistic conditions. For datasets that include additional covariates such as perturbation dose and time, we restrict the analysis to subsets with fixed conditions when applicable, as most existing models do not explicitly model these variables. This ensures a consistent evaluation setting across models and isolates perturbation-specific effects from confounding temporal or dosage variation. A summary of dataset characteristics and their benchmark roles is provided in Table 1.

**Unseen-cell generalization** We used McFarland2020 [36], a multiplexed drug-response dataset covering many cancer cell lines, and Kang2018\_CD4Tcells [37], which measures cytokine stimulation responses across multiple donors. These 2 datasets were selected to evaluate generalization across unseen cellular contexts at different levels, namely unseen cell lines and unseen patients.

**Unseen-perturbation generalization** We adopted 3 representative datasets in this setting. Norman2019 [38] was used for combinatorial genetic perturbation prediction, as it contains rich single- and dual-gene perturbation measurements. ReplogleWeissman2022\_K562 [11] was used

for large-scale single-gene perturbation prediction in a fixed cellular context. SrivatsanTrapnell2020\_sciplex3 [4] was used to benchmark generalization to unseen chemical perturbations.

**Cross-dataset integration** In this scenario, we chose AdamsonWeissman2016\_10X001, AdamsonWeissman2016\_10X010 [2], and ReplogleWeissman2022\_K562 [11]. The 2 Adamson datasets originate from the same study but differ in scale, which enables evaluation of same-study merging. ReplogleWeissman2022\_K562 provides a related but distinct large-scale CRISPR perturbation dataset in K562 cells, allowing us to further assess cross-study merging under heterogeneous experimental conditions.

## 4.2. Data Preprocessing

All datasets downloaded from scPerturb [35] were preprocessed using a unified pipeline implemented in Scanpy [50] and stored in the AnnData format [51]. The resulting processed datasets contained normalized log-expression values restricted to the selected highly variable genes, providing a standardized input representation for all benchmark models.

**Quality filtering** Cells with all-zero expression profiles were removed. Genes expressed in fewer than 10 cells were filtered out to eliminate extremely sparse features.

**Perturbation label processing** Cells lacking perturbation annotations were removed. Perturbation categories with zero cells were discarded, and categories containing fewer than 10 cells were filtered out to ensure reliable statistics. For datasets containing a large number of perturbations, only the top 500 perturbations ranked by cell count were retained.

**Normalization and transformation** Raw count matrices were stored in a separate layer and normalized using library-size normalization, scaling each cell to a total count of 10,000. The normalized counts were then log-transformed using a  $\log(1 + x)$  transformation.

**Highly variable gene selection** Highly variable genes (HVGs) were identified using the Seurat v3 method [46] implemented in Scanpy. The top 2,000 HVGs were selected for each dataset and used as the feature space for all downstream analyses.

**Perturbation filtering for embedding availability** For downstream modeling tasks requiring perturbation representations, perturbations without corresponding embeddings were removed. Specifically, perturbations not present in the precomputed protein sequence embeddings derived from ESM2 [52] or in the molecular fingerprint embeddings [53] were excluded. This filtering ensured that all perturbations retained in the dataset had valid embedding representations for subsequent model training and evaluation.

**Data splitting strategy** For single-perturbation tasks, cells were partitioned into training, validation, and test sets while maintaining balanced representation of control and perturbed cells. Control cells and perturbed cells were first independently divided into training and held-out subsets with a ratio of 4:1. The held-out subset was subsequently split evenly into validation and test sets. This procedure yielded a final split ratio of 8:1:1 for training, validation, and test sets, respectively.



For combination-perturbation tasks, we followed the dataset partitioning strategy outlined in the original GEARS paper [24]. The perturbed cells are split into 4 parts: Combo Unseen 0, Combo Unseen 1, Combo Unseen 2, Single Unseen 0, Single Unseen 1. For example, Combo Unseen 0 means 0 of the combination perturbations are not in the train-split perturbation sets. The train-split contains combo unseen 0 and single unseen 0. And the test-split includes Combo Unseen 0, Combo Unseen 1, Combo Unseen 2, and Single Unseen 1. We showed the results for each part of the test split.

For unseen-cell evaluation, splits were performed at the cell line or patient level to ensure that cells from the same biological source did not appear in multiple partitions. Under the random split setting, cell lines or patients were randomly assigned to the training, validation, and test sets using an approximate 8:1:1 ratio. When the total number of cell lines or patient categories was small, the number of categories in each split was adjusted proportionally to maintain sufficient samples in each subset. For embedding-based splits, cell lines or patients were first grouped into meta-clusters using representations derived from foundation models. These meta-clusters were then assigned to training and held-out partitions, ensuring that entire clusters were excluded from training. When only a small number of clusters were available, we used coarse partitions; for example, in Kang2018, three meta-clusters were identified, of which two were assigned to the training set and the remaining cluster was reserved for validation and test evaluation.

**Mask Mechanisms** To better fit the sparse distributions commonly observed in merged datasets, we optionally introduce a masking mechanism during training and evaluation.

During training, the loss is computed only on non-zero gene expressions to reduce the influence of excessive zeros. Instead of constructing a gene-level non-zero mask for each individual cell, we introduce a cell-class mask for multi-cell-line or merged datasets. Specifically, genes that are non-zero within a given cell class are identified and used to define the mask for that class.

During evaluation, we compute a cell-class-level mask based on the aggregated gene expression across all cells belonging to the same cell class. For each gene, expression values are first summed across cells within the class. Genes with non-zero aggregated expression are then retained in the mask for that cell class. Model performance is evaluated only on these masked genes, ensuring that evaluation focuses on genes with meaningful signal within the corresponding cell class. Finally, the evaluation metrics are averaged across all cell classes.

### 4.3. Benchmarked Models

We integrated 11 perturbation prediction models into the unified framework, spanning linear baselines, VAE-based generative models, geometric models, and embedding-based approaches (Table 2). All models were re-implemented under a shared input-output interface to ensure consistent preprocessing, data splitting, and evaluation, while preserving the core architecture of each original implementation. To enable fair comparison, we made minimal modifications to certain model-specific components to ensure compatibility with the unified evaluation pipeline, while keeping the underlying model formulations unchanged.

**Linear baselines** We include three linear baselines adapted from PerturBench [15]. **Linear Additive** predicts the perturbed expression as the sum of a control cell’s expression and a learnable perturbation-specific shift via a single linear layer. **Latent Additive** extends this by encoding both the control expression and perturbation identity into a shared latent space, where their additive combination is decoded back to gene expression via multilayer perceptrons. **DecoderOnly** predicts perturbed expression solely from perturbation and covariate identities without conditioning on control cell

expression, serving as a lower bound that simulates mode collapse.

**Deep learning models** We also include 8 deep Learning baselines:

**CPA** (Compositional Perturbation Autoencoder) [21] uses an adversarial VAE to disentangle basal cell state from perturbation effects, enabling compositional recombination of learned drug, dose, and cell-type embeddings for out-of-distribution prediction.

**BioLORD** [54] learns disentangled representations by partitioning the latent space into attribute-specific subspaces for known factors (e.g., perturbation, cell type) and an encoding of unknown variation, allowing counterfactual generation by recombining attribute embeddings.

**SAMS-VAE** [55] models perturbation effects as sparse additive shifts in latent space, where binary masks enforce perturbation-specific sparsity to promote disentangled and interpretable representations.

**GEARS** [24] integrates a gene co-expression graph and a Gene Ontology perturbation graph via dual graph neural networks, enabling extrapolation to unseen single and combinatorial genetic perturbations.

**PRnet** [56] is a perturbation-conditioned generative model pretrained on bulk transcriptomic data (LINCS L1000), which transfers pharmacological priors to predict single-cell responses to novel chemical perturbations.

**scLAMBDA** [57] combines a VAE architecture with LLM-derived biological priors for perturbation encoding, leveraging pretrained knowledge to improve generalization under limited single-cell training data.

**GenePert** [58] takes a minimalist approach, using gene embeddings as input features to a ridge regression model, demonstrating that rich text-based biological priors can outperform complex architectures on multiple perturbation prediction benchmarks.

**STATE** [59] is a set-based transformer architecture that predicts perturbation-induced state transitions by jointly modeling sets of cells via bidirectional self-attention, capturing both within-population heterogeneity and cross-context variation through a State Embedding module pretrained on observational data and a State Transition module trained on perturbation data.

Table 2 | Summary of benchmarked models. All models are evaluated under a unified interface with consistent preprocessing and evaluation protocols. GitHub links point to the original implementations from which each model was adapted.

Model	Category	Reference	Code
Linear Additive	Linear baseline	Wu et al. [15]	<a href="#">GitHub</a>
Latent Additive	Linear baseline	Wu et al. [15]	<a href="#">GitHub</a>
DecoderOnly	Linear baseline	Wu et al. [15]	<a href="#">GitHub</a>
CPA	Adversarial VAE	Lotfollahi et al. [21]	<a href="#">GitHub</a>
BioLORD	Disentanglement VAE	Piran et al. [54]	<a href="#">GitHub</a>
SAMS-VAE	Sparse additive VAE	Bereket & Karaletsos [55]	<a href="#">GitHub</a>
GEARS	Geometric model	Roohani et al. [24]	<a href="#">GitHub</a>
STATE	Set-based transformer	Adduri et al. [59]	<a href="#">GitHub</a>
PRnet	Pretrained generative	Qi et al. [56]	<a href="#">GitHub</a>
scLAMBDA	LLM-informed VAE	Wang et al. [57]	<a href="#">GitHub</a>
GenePert	LLM-embedding regression	Chen & Zou [58]	<a href="#">GitHub</a>

## 4.4. Evaluation Metrics

To systematically compare perturbation prediction models, we adopted a panel of 12 metrics organized into three complementary aspects: correlation-based measures, DEG-related scores, and distribution-level distances [35, 41]. Each metric is introduced below by its full descriptive name, with the abbreviated label used in all figures given in parentheses.

We first introduce notation. For perturbation  $p$ , let  $\mathbf{y}_p \in \mathbb{R}^G$  and  $\hat{\mathbf{y}}_p \in \mathbb{R}^G$  denote the observed and predicted mean expression profiles, respectively, where  $G$  is the number of genes. Let  $\mathbf{y}_0 \in \mathbb{R}^G$  denote the observed mean expression of control cells. For gene-level quantities,  $y_{p,g}$  and  $\hat{y}_{p,g}$  denote the  $g$ -th component of  $\mathbf{y}_p$  and  $\hat{\mathbf{y}}_p$ . For distribution-level metrics, let  $\hat{X}_p = \{\hat{\mathbf{x}}_i\}_{i=1}^n$  and  $X_p = \{\mathbf{x}_j\}_{j=1}^m$  denote the predicted and observed single-cell populations under perturbation  $p$ , respectively. All values are in log-normalized space.

### 4.4.1. Correlation-Based Measures

These metrics quantify gene-level agreement between predicted and true responses, capturing whether perturbation-induced expression changes are correctly ranked and directionally consistent.

**Pearson correlation (PCC)** PCC measures the linear agreement between the predicted and observed mean expression profiles:

$$\text{PCC}(p) = \text{corr}(\hat{\mathbf{y}}_p, \mathbf{y}_p). \quad (1)$$

**Perturbation-delta correlation (PDCorr)** PDCorr computes the Pearson correlation on perturbation-induced changes rather than raw expression levels. The predicted and observed deltas relative to the control baseline are defined as

$$\Delta \hat{\mathbf{y}}_p = \hat{\mathbf{y}}_p - \mathbf{y}_0, \quad \Delta \mathbf{y}_p = \mathbf{y}_p - \mathbf{y}_0. \quad (2)$$

PDCorr is then defined as

$$\text{PDCorr}(p) = \text{corr}(\Delta \hat{\mathbf{y}}_p, \Delta \mathbf{y}_p). \quad (3)$$

By removing the shared control profile, this metric isolates the perturbation-specific signal from the baseline expression level [24, 26].

**Spearman correlation of log-fold-change (LFCspear)** LFCspear measures rank-order concordance between predicted and observed gene-level fold changes. For gene  $g$ , the predicted and observed log-fold-changes are

$$\widehat{\text{lfc}}_{p,g} = \log_2(\hat{y}_{p,g} + \epsilon) - \log_2(y_{0,g} + \epsilon), \quad \text{lfc}_{p,g} = \log_2(y_{p,g} + \epsilon) - \log_2(y_{0,g} + \epsilon), \quad (4)$$

where  $\epsilon = 0.1$  is a pseudocount. The metric is defined as

$$\text{LFCspear}(p) = \text{Spearman}(\widehat{\text{lfc}}_p, \text{lfc}_p). \quad (5)$$

**PCA Spearman correlation of log-fold-change (PCA-LFCspear)** PCA-LFCspear is computed identically to LFCspear after projecting the fold-change vectors into a 50-dimensional PCA space fitted on the reference data, thereby reducing noise and emphasizing large-scale structured variation.

**Cosine similarity of log-fold-change (LogFC)** LogFC measures the directional agreement between predicted and observed fold-change profiles:

$$\text{LogFC}(p) = \frac{\widehat{\text{lf}}_p \cdot \text{lf}_p}{\|\widehat{\text{lf}}_p\|_2 \|\text{lf}_p\|_2}. \quad (6)$$

**Rank of cosine log-fold-change (RLogFC)** RLogFC assesses whether a model preserves perturbation identity rather than merely recovering average trends. For each test perturbation  $p$ , the predicted fold-change profile is compared against the observed fold-change profiles of all  $N$  test perturbations using cosine similarity, and the rank of the true match is recorded. The normalized rank is defined as

$$\text{RLogFC}(p) = \frac{r(p) - 1}{N - 1}, \quad (7)$$

where  $r(p)$  is the position of the true perturbation when all candidates are sorted by descending cosine similarity. A value of 0 indicates perfect identification; a value near 0.5 corresponds to random ordering.

#### 4.4.2. DEG-Related Scores

These metrics evaluate the recovery of differentially expressed genes, which are central to biological interpretation in perturbation experiments. For each perturbation  $p$ , the top 50 DEGs are identified by absolute expression change from control in the predicted and observed profiles, respectively:

$$\widehat{\mathcal{D}}_p = \text{Top-50}(|\hat{y}_{p,g} - y_{0,g}|), \quad \mathcal{D}_p = \text{Top-50}(|y_{p,g} - y_{0,g}|). \quad (8)$$

**Top-50 DEG precision (DEPrec)** DEPrec measures the fraction of predicted top-50 DEGs that are among the true top-50 DEGs:

$$\text{DEPrec}(p) = \frac{|\widehat{\mathcal{D}}_p \cap \mathcal{D}_p|}{|\widehat{\mathcal{D}}_p|}. \quad (9)$$

**Top-50 DEG recall (DERec)** DERec measures the fraction of true top-50 DEGs that are recovered by the predicted top-50 DEGs:

$$\text{DERec}(p) = \frac{|\widehat{\mathcal{D}}_p \cap \mathcal{D}_p|}{|\mathcal{D}_p|}. \quad (10)$$

**Top-50 DEG overlap (DEOverlap)** DEOverlap quantifies the agreement between predicted and true top-50 DEG sets using the Jaccard index:

$$\text{DEOverlap}(p) = \frac{|\widehat{\mathcal{D}}_p \cap \mathcal{D}_p|}{|\widehat{\mathcal{D}}_p \cup \mathcal{D}_p|}. \quad (11)$$

#### 4.4.3. Distribution-Level Distances

These metrics assess whether the predicted cellular state matches the global shift in expression space induced by perturbations, beyond population-average agreement.

**Root mean squared error (RMSE)** RMSE quantifies the average magnitude of prediction error across genes:

$$\text{RMSE}(p) = \sqrt{\frac{1}{G} \|\hat{\mathbf{y}}_p - \mathbf{y}_p\|_2^2}. \quad (12)$$

Unlike correlation-based metrics, RMSE is sensitive to both the direction and the absolute scale of prediction errors.

**Energy distance (ED)** Energy distance [40] quantifies the discrepancy between the predicted and observed single-cell distributions:

$$\text{ED}(\hat{X}_p, X_p) = \frac{2}{nm} \sum_{i=1}^n \sum_{j=1}^m \|\hat{\mathbf{x}}_i - \mathbf{x}_j\|_2 - \frac{1}{n^2} \sum_{i=1}^n \sum_{i'=1}^n \|\hat{\mathbf{x}}_i - \hat{\mathbf{x}}_{i'}\|_2 - \frac{1}{m^2} \sum_{j=1}^m \sum_{j'=1}^m \|\mathbf{x}_j - \mathbf{x}_{j'}\|_2. \quad (13)$$

A value of zero indicates identical distributions; larger values indicate greater discrepancy.

**Sinkhorn divergence (SD)** Sinkhorn divergence [60] provides an entropically regularized optimal-transport measure between the predicted and observed single-cell populations. Given a cost function  $c(\mathbf{x}, \mathbf{y}) = \|\mathbf{x} - \mathbf{y}\|_2^2$  and regularization parameter  $\varepsilon > 0$ , the debiased Sinkhorn divergence is defined as

$$\text{SD}(\hat{X}_p, X_p) = \text{OT}_\varepsilon(\hat{X}_p, X_p) - \frac{1}{2} \text{OT}_\varepsilon(\hat{X}_p, \hat{X}_p) - \frac{1}{2} \text{OT}_\varepsilon(X_p, X_p), \quad (14)$$

where  $\text{OT}_\varepsilon$  denotes the entropy-regularized optimal transport cost. We compute SD using the GeomLoss library [61] with  $\varepsilon = 0.05$ .

**PCA Sinkhorn divergence (PCA-SD)** PCA-SD applies the same Sinkhorn computation after projecting cells into a 50-dimensional PCA space fitted on the reference data, reducing computational cost and noise sensitivity.

**Computational resources** Most model training and inference experiments were conducted on an Ubuntu 18.04 system equipped with 8 NVIDIA GeForce RTX 4090 GPUs and large system memory. Memory-intensive tasks, including foundation model-based approaches and certain preprocessing analyses, were performed on a separate server with NVIDIA A800-SXM4-80GB GPUs (80 GB memory per GPU). All experiments used consistent preprocessing and evaluation protocols to ensure fair comparison across models.

**Data availability** All datasets used in this study are derived from the scPerturb resource, which provides uniformly processed single-cell perturbation data in AnnData (h5ad) format [35]. The data are publicly available at <https://zenodo.org/records/13350497>.

Based on these datasets, we performed additional preprocessing to construct task-specific splits for benchmarking, including unseen cell, unseen perturbation, and cross-dataset integration scenarios. The processed datasets corresponding to these tasks are available at [https://drive.google.com/drive/folders/1GrPW9x5\\_npnT7ILwDVsfWvfdIcqaSjdk?usp=sharing](https://drive.google.com/drive/folders/1GrPW9x5_npnT7ILwDVsfWvfdIcqaSjdk?usp=sharing).

All data are provided in standard formats with accompanying metadata to facilitate reproducibility.

**Code availability** Unlike prior works, our framework offers a unified data pipeline for all models, thereby eliminating the influence of data-pipeline discrepancies and enabling fair comparisons. The framework is also designed for easy integration of new models into the unified benchmark. To help users get started, we provide a running tutorial for the Unseen Perturbation task as an example of code usage. The code is available at <https://github.com/maoxinjie/VCBench/>. We also provide an interactive web-based demo to facilitate exploration of the benchmark results and model comparisons at <https://maoxinjie.github.io/VCBench-demo/>.

## References

- [1] Atray Dixit, Oren Parnas, Biyu Li, Jenny Chen, Charles P Fulco, Livnat Jerby-Arnon, Nemanja D Marjanovic, Danielle Dionne, Tyler Burks, Raktima Raychowdhury, et al. Perturb-seq: dissecting molecular circuits with scalable single-cell rna profiling of pooled genetic screens. *cell*, 167(7): 1853–1866, 2016.
- [2] Britt Adamson, Thomas M Norman, Marco Jost, Min Y Cho, James K Nuñez, Yuwen Chen, Jacqueline E Villalta, Luke A Gilbert, Max A Horlbeck, Marco Y Hein, et al. A multiplexed single-cell crispr screening platform enables systematic dissection of the unfolded protein response. *Cell*, 167(7):1867–1882, 2016.
- [3] Paul Datlinger, André F Rendeiro, Christian Schmidl, Thomas Krausgruber, Peter Traxler, Johanna Klughammer, Linda C Schuster, Amelie Kuchler, Donat Alpar, and Christoph Bock. Pooled crispr screening with single-cell transcriptome readout. *Nature methods*, 14(3):297–301, 2017.
- [4] Sanjay R Srivatsan, José L McFaline-Figueroa, Vijay Ramani, Lauren Saunders, Junyue Cao, Jonathan Packer, Hannah A Pliner, Dana L Jackson, Riza M Daza, Lena Christiansen, et al. Massively multiplex chemical transcriptomics at single-cell resolution. *Science*, 367(6473): 45–51, 2020.
- [5] Ophir Shalem, Neville E Sanjana, Ella Hartenian, Xi Shi, David A Scott, Tarjei S Mikkelsen, Dirk Heckl, Benjamin L Ebert, David E Root, John G Doench, and Feng Zhang. Genome-scale crispr-cas9 knockout screening in human cells. *Science*, 343(6166):84–87, 2014.
- [6] Christoph Bock, Paul Datlinger, Florence Chardon, Matthew A Coelho, Matthew B Dong, Keith A Lawson, Tian Lu, Laetitia Maroc, Thomas M Norman, Bicna Song, et al. High-content crispr screening. *Nature Reviews Methods Primers*, 2(1):8, 2022.
- [7] Raphael Petegrosso, Zhuliu Li, and Rui Kuang. Machine learning and statistical methods for clustering single-cell rna-sequencing data. *Briefings in bioinformatics*, 21(4):1209–1223, 2020.
- [8] Kenji Kamimoto, Blerta Stringa, Christy M Hoffmann, Kunal Jindal, Lilianna Solnica-Krezel, and Samantha A Morris. Dissecting cell identity via network inference and in silico gene perturbation. *Nature*, 614(7949):742–751, 2023.
- [9] Bram Van de Sande, Joon Sang Lee, Euphemia Mutasa-Gottgens, Bart Naughton, Wendi Bacon, Jonathan Manning, Yong Wang, Jack Pollard, Melissa Mendez, Jon Hill, et al. Applications of single-cell rna sequencing in drug discovery and development. *Nature Reviews Drug Discovery*, 22(6):496–520, 2023.
- [10] Jean-Louis Reymond. The chemical space project. *Accounts of Chemical Research*, 48(3):722–730, 2015.

- 
- [11] Joseph M Replogle, Reuben A Saunders, Angela N Pogson, Jeffrey A Hussmann, Alexander Lenail, Alina Guna, Lauren Mascibroda, Eric J Wagner, Karen Adelman, Gila Lithwick-Yanai, et al. Mapping information-rich genotype-phenotype landscapes with genome-scale perturb-seq. *Cell*, 185(14):2559–2575, 2022.
- [12] George I Gavriilidis, Vasileios Vasileiou, Aspasia Orfanou, Naveed Ishaque, and Fotis Psomopoulos. A mini-review on perturbation modelling across single-cell omic modalities. *Computational and Structural Biotechnology Journal*, 23:1886–1896, 2024.
- [13] Jennifer E Rood, Aleksandra Hupalowska, and Aviv Regev. Toward a foundation model of causal cell and tissue biology with a perturbation cell and tissue atlas. *Cell*, 187(17):4520–4545, 2024.
- [14] Zhiting Wei, Yiheng Wang, Yicheng Gao, Shuguang Wang, Ping Li, Duanmiao Si, Yuli Gao, Siqi Wu, Danlu Li, Kejing Dong, et al. Benchmarking algorithms for generalizable single-cell perturbation response prediction. *Nature Methods*, 23(2):451–464, 2026.
- [15] Yan Wu, Esther Wershof, Sebastian M Schmon, Marcel Nassar, Błażej Osiński, Ridvan Eksi, Zichao Yan, Rory Stark, Kun Zhang, and Thore Graepel. Perturbench: Benchmarking machine learning models for cellular perturbation analysis. *arXiv preprint arXiv:2408.10609*, 2024.
- [16] Constantin Ahlmann-Eltze, Wolfgang Huber, and Simon Anders. Deep-learning-based gene perturbation effect prediction does not yet outperform simple linear baselines. *Nature Methods*, 22:1657–1661, 2025.
- [17] Daniel R Wong, Abby S Hill, and Rob Moccia. Simple controls exceed best deep learning algorithms and reveal foundation model effectiveness for predicting genetic perturbations. *Bioinformatics*, 41(6):btaf317, 2025.
- [18] Mohammad Lotfollahi, F Alexander Wolf, and Fabian J Theis. scgen predicts single-cell perturbation responses. *Nature methods*, 16(8):715–721, 2019.
- [19] Romain Lopez, Jeffrey Regier, Michael B Cole, Michael I Jordan, and Nir Yosef. Deep generative modeling for single-cell transcriptomics. *Nature methods*, 15(12):1053–1058, 2018.
- [20] Mohammad Lotfollahi, Mohsen Naghipourfar, Fabian J Theis, and F Alexander Wolf. Conditional out-of-distribution generation for unpaired data using transfer vae. *Bioinformatics*, 36(Supplement\_2):i610–i617, 2020.
- [21] Mohammad Lotfollahi, Anna Klimovskaia Susmelj, Carlo De Donno, Leon Hetzel, Yuge Ji, Ignacio L Ibarra, Sanjay R Srivatsan, Mohsen Naghipourfar, Riza M Daza, Beth Martin, et al. Predicting cellular responses to complex perturbations in high-throughput screens. *Molecular systems biology*, 19(6):MSB202211517, 2023.
- [22] Charlotte Bunne, Stefan G Stark, Gabriele Gut, Jacobo Sarabia del Castillo, Mitch Levesque, Kjong-Van Lehmann, Lucas Pelkmans, Andreas Krause, and Gunnar Rätsch. Learning single-cell perturbation responses using neural optimal transport. *Nature Methods*, 20(11):1759–1768, 2023.
- [23] Dominik Klein, Jonas Simon Fleck, Dmitrii Bobrovskiy, Leander Zimmermann, Simon Becker, Alessandro Palma, Leander Dony, Alejandro Tejada-Lapuerta, Guillaume Hugué, Hsiu-Chuan Lin, et al. Cellflow enables generative single-cell phenotype modeling with flow matching. *bioRxiv*, 2025.
- [24] Yusuf Roohani, Kexin Huang, and Jure Leskovec. Predicting transcriptional outcomes of novel multigene perturbations with gears. *Nature Biotechnology*, 42(6):927–935, 2024.
-

- [25] Siyu He, Yuefei Zhu, Daniel Naveed Tavakol, Haotian Ye, Yeh-Hsing Lao, Zixian Zhu, Cong Xu, Shradha Chauhan, Guy Garty, Raju Tomer, et al. Squidiff: predicting cellular development and responses to perturbations using a diffusion model. *Nature Methods*, 23(1):65–77, 2026.
- [26] Haotian Cui, Chloe Wang, Hassaan Maan, Kuan Pang, Fengning Luo, Nan Duan, and Bo Wang. scgpt: toward building a foundation model for single-cell multi-omics using generative ai. *Nature methods*, 21(8):1470–1480, 2024.
- [27] Minsheng Hao, Jing Gong, Xin Zeng, Chiming Liu, Yucheng Guo, Xingyi Cheng, Taifeng Wang, Jianzhu Ma, Le Song, and Xuegong Zhang. Large-scale foundation model on single-cell transcriptomics. *Nature Methods*, 21(8):1481–1491, 2024.
- [28] Christina V Theodoris, Ling Xiao, Anant Chopra, Mark D Chaffin, Zeina R Al Sayed, Matthew C Hill, Helene Mantineo, Elizabeth M Brydon, Zexian Zeng, X Shirley Liu, et al. Transfer learning enables predictions in network biology. *Nature*, 618(7965):616–624, 2023.
- [29] Fan Yang, Wenchuan Wang, Fang Wang, Yuan Fang, Duyu Tang, Junzhou Huang, Hui Lu, and Jianhua Yao. scbert as a large-scale pretrained deep language model for cell type annotation of single-cell rna-seq data. *Nature Machine Intelligence*, 4(10):852–866, 2022.
- [30] Gerold Csentes, Gema Sanz, Kristóf Z Szalay, and Bence Szalai. Benchmarking foundation cell models for post-perturbation rna-seq prediction. *BMC genomics*, 26(1):393, 2025.
- [31] Aaron Wenteler, Martina Occhetta, Nikhil Branson, Magdalena Huebner, Victor Curean, WT Dee, WT Connell, Alex Hawkins-Hooker, Siu Pui Chung, Yasha Ektefaie, et al. Perteval-scfm: benchmarking single-cell foundation models for perturbation effect prediction. *BioRxiv*, pages 2024–10, 2024.
- [32] Eric Kernfeld, Yunxiao Yang, Joshua S Weinstock, Alexis Battle, and Patrick Cahan. A systematic comparison of computational methods for expression forecasting. *bioRxiv*, 2023.
- [33] Daniel Burkhardt, Andrew Benz, Robrecht Cannoodt, Mauricio Cortes, Scott Gigante, Christopher Lance, Richard Lieberman, Malte Luecken, and Angela Pisco. Single-cell perturbation prediction: generalizing experimental interventions to unseen contexts. In *NeurIPS Competition Track*, 2023.
- [34] Ihab Bendidi et al. Benchmarking transcriptomics foundation models for perturbation analysis: one pca still rules them all. *arXiv preprint arXiv:2410.13956*, 2024.
- [35] Stefan Peidli, Tessa D Green, Ciyue Shen, Torsten Gross, Joseph Min, Samuele Garda, Bo Yuan, Linus J Schumacher, Jake P Taylor-King, Debora S Marks, et al. scperturb: harmonized single-cell perturbation data. *Nature Methods*, 21(3):531–540, 2024.
- [36] James M McFarland, Brenton R Paoletta, Allison Warren, Kathryn Geiger-Schuller, Tsukasa Shibue, Michael Rothberg, Olena Kuksenko, William N Colgan, Andrew Jones, Emily Chambers, et al. Multiplexed single-cell transcriptional response profiling to define cancer vulnerabilities and therapeutic mechanism of action. *Nature communications*, 11(1):4296, 2020.
- [37] Hyun Min Kang, Meena Subramaniam, Sasha Targ, Michelle Nguyen, Lenka Maliskova, Elizabeth McCarthy, Eunice Wan, Simon Wong, Lauren Byrnes, Cristina M Lanata, et al. Multiplexed droplet single-cell rna-sequencing using natural genetic variation. *Nature biotechnology*, 36(1): 89–94, 2018.



- [38] Thomas M Norman, Max A Horlbeck, Joseph M Replogle, Alex Y Ge, Albert Xu, Marco Jost, Luke A Gilbert, and Jonathan S Weissman. Exploring genetic interaction manifolds constructed from rich single-cell phenotypes. *Science*, 365(6455):786–793, 2019.
- [39] Arthur Gretton, Karsten M Borgwardt, Malte J Rasch, Bernhard Schölkopf, and Alexander Smola. A kernel two-sample test. *Journal of Machine Learning Research*, 13(25):723–773, 2012.
- [40] Gábor J Székely and Maria L Rizzo. Energy statistics: A class of statistics based on distances. *Journal of Statistical Planning and Inference*, 143(8):1249–1272, 2013.
- [41] Yuge Ji, Tessa D Green, Stefan Peidli, Mojtaba Bahrami, Meiqi Liu, Luke Zappia, Karin Hrovatin, Chris Sander, and Fabian J Theis. Optimal distance metrics for single-cell rna-seq populations. *bioRxiv*, pages 2023–12, 2023.
- [42] Qun Jiang, Shengquan Chen, Xiaoyang Chen, and Rui Jiang. scpram accurately predicts single-cell gene expression perturbation response based on attention mechanism. *Bioinformatics*, 40(5):btac265, 2024.
- [43] Malte D Luecken, Maren Büttner, Kridsakorn Chaichoompu, Anna Danese, Marta Interlandi, Michaela F Müller, Daniel C Strobl, Luke Zappia, Martin Dugas, Maria Colomé-Tatché, and Fabian J Theis. Benchmarking atlas-level data integration in single-cell genomics. *Nature Methods*, 19(1):41–50, 2022.
- [44] Jared Kaplan, Sam McCandlish, Tom Henighan, Tom B Brown, Benjamin Chess, Rewon Child, Scott Gray, Alec Radford, Jeffrey Wu, and Dario Amodei. Scaling laws for neural language models. *arXiv preprint arXiv:2001.08361*, 2020.
- [45] Leon Hetzel, Simon Boehm, Niki Kilbertus, Stephan Günemann, and Fabian Theis. Predicting cellular responses to novel drug perturbations at a single-cell resolution. *Advances in Neural Information Processing Systems*, 35:26711–26722, 2022.
- [46] Tim Stuart, Andrew Butler, Paul Hoffman, Christoph Hafemeister, Efthymia Papalexi, William M Mauck, Yuhan Hao, Marlon Stoeckius, Peter Smibert, and Rahul Satija. Comprehensive integration of single-cell data. *cell*, 177(7):1888–1902, 2019.
- [47] Jesse Zhang, Ariel A Ubas, Roger de Borja, Valentine Svensson, Nathan Thomas, Noopur Thakar, et al. Tahoe-100m: A giga-scale single-cell perturbation atlas for context-dependent gene function and cellular modeling. *bioRxiv*, 2025.
- [48] Alex C Huang et al. X-atlas/orion: Genome-wide perturb-seq datasets via a scalable fix-cryopreserve platform for training dose-dependent biological foundation models. *bioRxiv*, 2025.
- [49] Alexander Rives, Joshua Meier, Tom Sercu, Siddharth Goyal, Zeming Lin, Jason Liu, Demi Guo, Myle Ott, C Lawrence Zitnick, Jerry Ma, and Rob Fergus. Biological structure and function emerge from scaling unsupervised learning to 250 million protein sequences. *Proceedings of the National Academy of Sciences*, 118(15):e2016239118, 2021.
- [50] F Alexander Wolf, Philipp Angerer, and Fabian J Theis. Scanpy: large-scale single-cell gene expression data analysis. *Genome biology*, 19(1):15, 2018.
- [51] Isaac Virshup, Sergei Rybakov, Fabian J Theis, Philipp Angerer, and F Alexander Wolf. anndata: Annotated data. *BioRxiv*, pages 2021–12, 2021.

- 
- [52] Zeming Lin, Halil Akin, Roshan Rao, Brian Hie, Zhongkai Zhu, Wenting Lu, Nikita Smetanin, Robert Verkuil, Ori Kabeli, Yaniv Shmueli, et al. Evolutionary-scale prediction of atomic-level protein structure with a language model. *Science*, 379(6637):1123–1130, 2023.
- [53] David Rogers and Mathew Hahn. Extended-connectivity fingerprints. *Journal of chemical information and modeling*, 50(5):742–754, 2010.
- [54] Zoe Piran, Niv Cohen, Yedid Hoshen, and Mor Nitzan. Disentanglement of single-cell data with biolord. *Nature Biotechnology*, 42(11):1678–1683, 2024.
- [55] Michael Bereket and Theofanis Karaletsos. Modelling cellular perturbations with the sparse additive mechanism shift variational autoencoder. *Advances in Neural Information Processing Systems*, 36:1–12, 2023.
- [56] Xiaoning Qi, Lianhe Zhao, Chenyu Tian, Yueyue Li, Zhen-Lin Chen, Peipei Huo, Runsheng Chen, Xiaodong Liu, Baoping Wan, Shengyong Yang, and Yi Zhao. Predicting transcriptional responses to novel chemical perturbations using deep generative model for drug discovery. *Nature Communications*, 15(1):9256, 2024.
- [57] Gefei Wang, Tianyu Liu, Jia Zhao, Youshu Cheng, and Hongyu Zhao. Modeling and predicting single-cell multi-gene perturbation responses with sclambda. *bioRxiv*, 2024.
- [58] Yiqun T Chen and James Zou. Genepert: Leveraging genept embeddings for gene perturbation prediction. *bioRxiv*, 2024.
- [59] Abhinav K Adduri, Dhruv Gautam, Beatrice Bevilacqua, Alishba Imran, Rohan Shah, Mohsen Naghipourfar, Noam Teyssier, Rajesh Ilango, Sanjay Nagaraj, Mingze Dong, et al. Predicting cellular responses to perturbation across diverse contexts with state. *bioRxiv*, 2025.
- [60] Marco Cuturi. Sinkhorn distances: Lightspeed computation of optimal transport. *Advances in neural information processing systems*, 26, 2013.
- [61] Jean Feydy, Thibault Séjourné, François-Xavier Vialard, Shun-ichi Amari, Alain Trounev, and Gabriel Peyré. Interpolating between optimal transport and mmd using sinkhorn divergences. In *The 22nd international conference on artificial intelligence and statistics*, pages 2681–2690. PMLR, 2019.



Figure S1 | **Hierarchical clustering of cell lines based on STACK embeddings in the McFarland2020 dataset.** Cell lines are embedded using the STACK foundation model and clustered using cosine distance. The resulting hierarchy is partitioned into 10 meta-clusters, which are used to define cell-state-based splits for unseen-cell generalization.

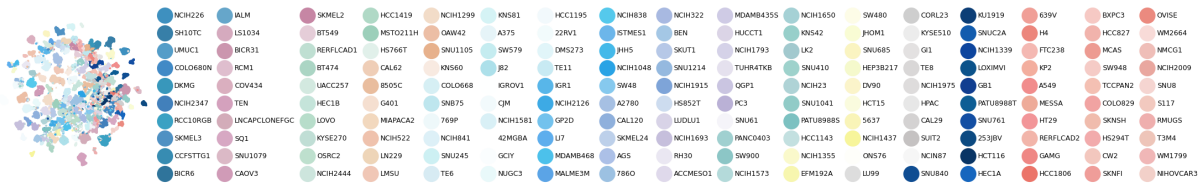


Figure S2 | **Visualization of all cell line distribution in the McFarlandTsherniak2020 dataset.** UMAP projection of cells colored by cell line identity. Each point represents a single cell, and colors indicate distinct cell lines.

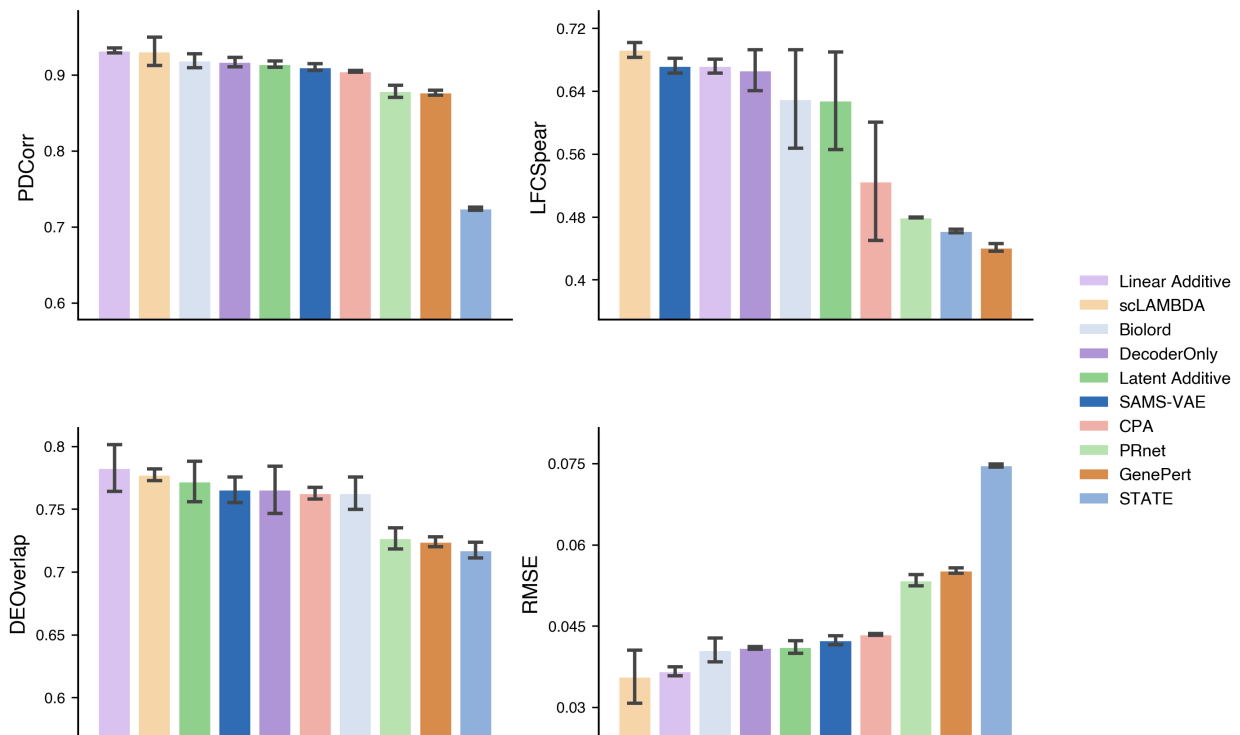


Figure S3 | **Performance comparison of perturbation prediction models on the Kang2018 dataset without cell embedding.** Results are evaluated using four metrics:  $\Delta$ PCC, Spearman correlation of log fold change, DEG overlap, and RMSE. Each bar represents the mean performance across runs, and error bars indicate standard deviation.

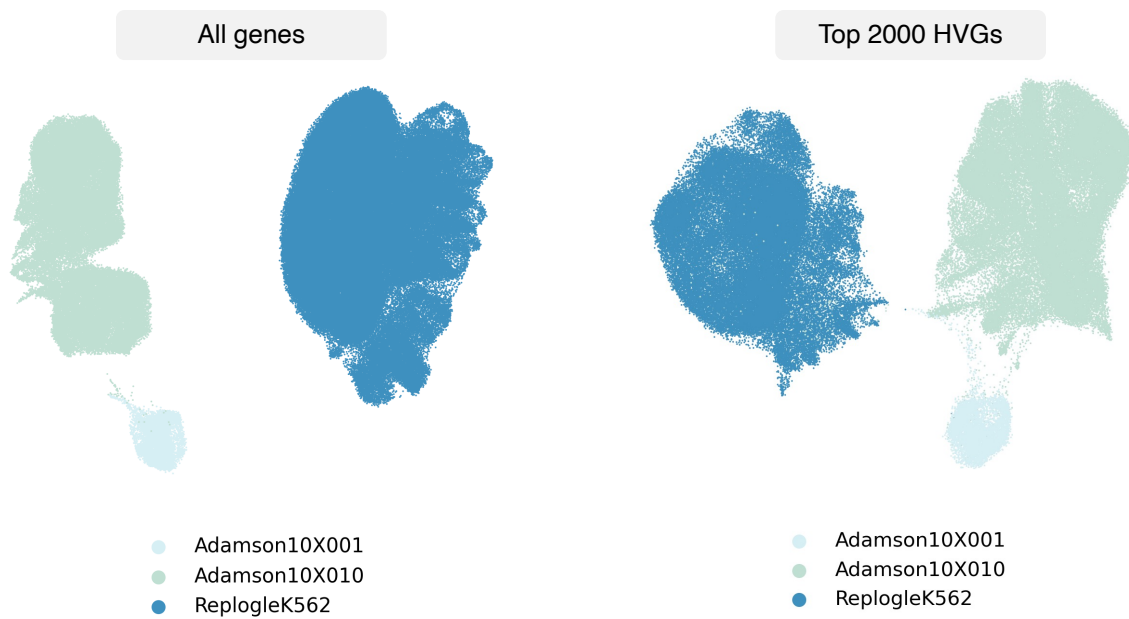


Figure S4 | **Effect of feature selection on cross-dataset structure.** UMAP visualization of cells from three K562 datasets (Adamson10X001, Adamson10X010, and ReplogleK562) under different feature spaces. UMAP computed using all genes (left) and UMAP computed using the top 2000 highly variable genes (right).

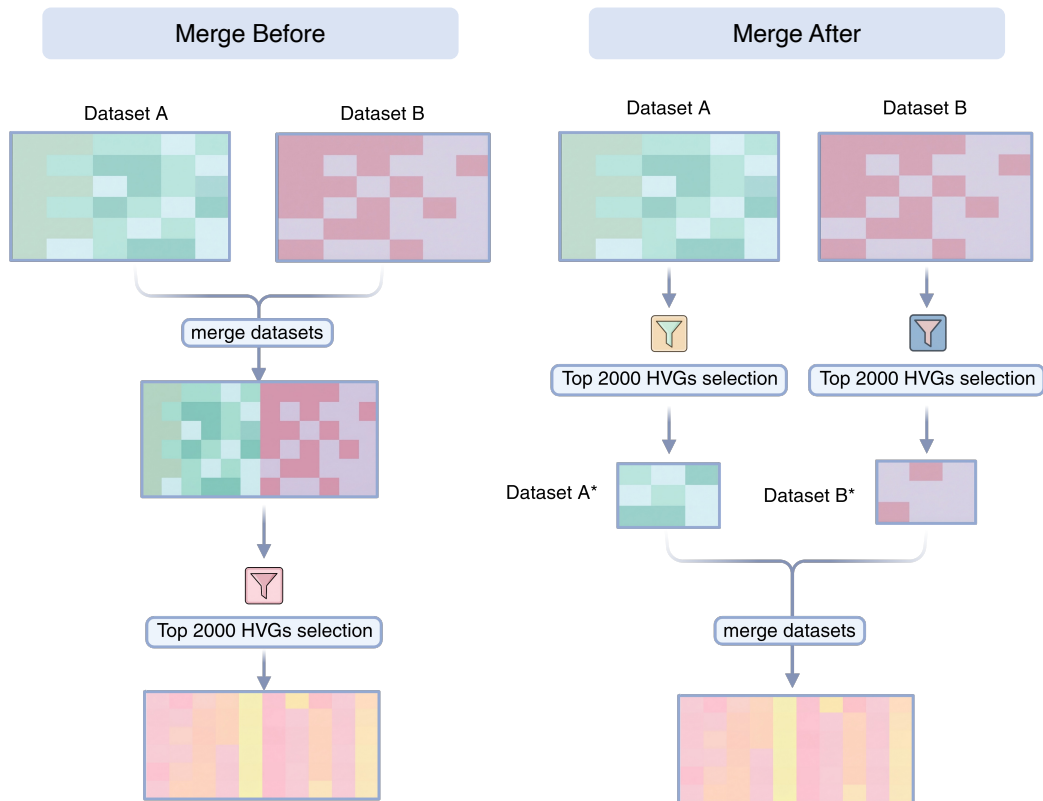


Figure S5 | **Illustration of dataset integration strategies.** Two alternative pipelines for integrating multiple datasets are shown. In the *merge-before* strategy (left), datasets are concatenated prior to feature selection, and highly variable genes (HVGs) are selected from the merged data. In the *merge-after* strategy (right), HVGs are first selected independently within each dataset, and the resulting feature spaces are then combined during dataset integration.